AMERICAN JOURNAL OF MANAGEMENT AND IOT MEDICAL COMPUTING
Peer Reviewed, Referred & Indexed Journal
E-ISSN: 3069-0110
Vol.5, No.4 (2026)
www.ajmimc.com

ANN-BASED SUPERVISORY CONTROL OF VEHICLE-TO-GRID TECHNOLOGY IN A MICROGRID USING DC FAST CHARGING ARCHITECTURE

ALLUMALLA.RAM PRASAD [1], Y. NAVEEN KUMAR [2]

[1] Student, Department of Electrical and Electronics Engineering, Sanketika Vidya Parishad Engineering College, Pothinamallayya Palem (P.M. Palem), Visakhapatnam, Andhra Pradesh, India– 530041 Email: allumallaramprasad3@gmail.com

[2] Assistant Professor, Department of Electrical and Electronics Engineering, Sanketika Vidya Parishad Engineering College, Pothinamallayya Palem (P.M. Palem), Visakhapatnam, Andhra Pradesh, India– 530041 Email: svpec.naveen2666@gmail.com

ABSTRACT

Electric vehicle (EV) batteries can act as energy storage in micro-grids by charging when there is surplus generation (grid-to-vehicle, G2V) and returning energy when it is needed (vehicle-to-grid, V2G). Mohammed Shakeel and Malik proposed a DC fast-charging station for V2G in a grid-connected micro-grid, in which four EVs and a 50 kW photovoltaic array share a 1.5 kV DC bus that is connected to the micro-grid through a 250 kVA grid-connected inverter with an LCL filter. In that work the battery chargers and the inverter use fixed-gain proportional–integral (PI) controllers, which produce DC-bus voltage spikes of 40–65 V and battery-current overshoot of about 11 % whenever an EV changes mode. This thesis replaces every PI regulator of the station — the constant-current loops of the off-board chargers and the dq current and DC-voltage loops of the inverter — with an artificial neural network (ANN) controller. Each ANN is a 3–10–1 multilayer perceptron whose inputs are the error, its integral and its derivative, and it slots into the original control structure without changing the feed-forward, decoupling or modulation stages. A two-stage training method is proposed: the networks are first fitted to the PI law with the Levenberg–Marquardt algorithm, giving a stable starting point, and are then optimised in closed loop with an evolution strategy on a station model that includes computation delay and sensor noise. A PI controller re-tuned on the same objective is used as an additional benchmark.

Simulation studies covering the base-paper V2G–G2V scenario, PV variation, four simultaneous EVs, parameter variation, grid voltage sag, power quality and sensor noise show that, compared with the base-paper PI, the ANN reduces the DC-bus voltage deviation by 20–29 %, roughly halves the DC-bus settling time, lowers the ITAE by 64 %, cuts battery-current overshoot to 2–5 % and reduces inverter modulation noise by 60 %. The optimised PI benchmark achieves nearly the same dynamics, so the benefit specific to the ANN structure is modest. The ANN also gives higher grid-current THD than the base PI (1.08 % against 0.74 % under base-paper conditions, but 5.82 % against 4.24 % with dead time) and loses part of its advantage under combined parameter variation. These limitations, and the remedies proposed for them, are discussed.

AMERICAN JOURNAL OF MANAGEMENT AND IOT MEDICAL COMPUTING
Peer Reviewed, Referred & Indexed Journal
E-ISSN: 3069-0110
Vol.5, No.4 (2026)
www.ajmimc.com

Keywords: Artificial neural network, DC fast charging, electric vehicle, grid-connected inverter, micro-grid, off-board charger, PI controller, vehicle-to-grid.

1. INTRODUCTION

1.1 Background

Transport electrification is one of the most significant changes taking place in modern power systems. Global sales of electric cars have grown rapidly over the last decade, and electric vehicles (EVs) are expected to form a large share of the passenger fleet within the next two decades [1]. Each EV carries a traction battery of typically 40–100 kWh, which is far larger than the storage installed in most homes and small commercial buildings. At the same time, the share of wind and solar photovoltaic (PV) generation in distribution networks is increasing. These sources are variable and only partly predictable, so the networks that host them need flexible storage and fast-acting power-electronic interfaces to keep supply and demand balanced.

A micro-grid is a cluster of distributed generators, storage devices and loads that can operate either connected to the utility grid or as an autonomous island [2], [3]. Within a micro-grid, energy storage is essential: it absorbs surplus renewable generation, supplies energy during deficits and supports voltage and frequency. Dedicated stationary batteries are expensive, whereas privately owned EVs are already present and, on average, sit parked for about 22 hours a day [4]. When an EV is plugged into a bidirectional charger, its battery can act as a distributed storage asset for the micro-grid. This is the basic idea behind vehicle-to-grid (V2G) technology.

1.2 Electric Vehicle Charging Levels

The Society of Automotive Engineers (SAE) classifies conductive EV charging into three levels [5], [6], summarised in Table 1.1 and illustrated in Fig. 1.1. Level 1 and Level 2 are AC charging methods: the vehicle's on-board charger converts the AC supply to DC, so the available power is limited by the rating of that on-board converter. Level 3, or DC fast charging, uses an off-board charger housed in the electric vehicle supply equipment (EVSE) and supplies DC power directly to the battery at up to 90 kW and above, cutting charging time to roughly 20–30 minutes [7].

Table 1.1 SAE charging levels (after [5], [6], [7])

Level	Supply	Typical power	Charger location / remarks
Level 1	120 V AC, single phase	1.4–1.9 kW	On-board; overnight home charging, < 60 km/day
Level 2	208–240 V AC, up to 30 A	3.3–7.2 kW	On-board; dedicated home or public EVSE
Level 3 (DC fast)	200–450 V DC	up to 90 kW	Off-board in EVSE; 20–30 min charge; suits V2G

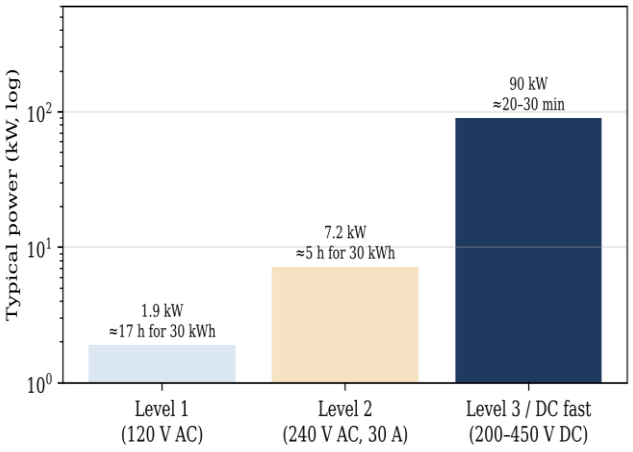


Fig. 1.1 Typical charging power of the three SAE charging levels (logarithmic scale)

For V2G in a micro-grid, DC fast charging has two practical advantages. First, high-power off-board chargers can exchange tens of kilowatts quickly, which is what storage duty in a micro-grid demands. Second, the common DC bus of a fast-charging station can also host DC sources such as a PV array, so that one grid-connected inverter serves both the vehicles and the renewable source [7].

2.LITERATURE REVIEW

2.1 Introduction

This chapter reviews the published work relevant to the thesis in four areas: V2G technology and its grid services; charger topologies and fast-charging station architectures; control of grid-connected voltage-source converters; and intelligent, in particular neural-network, control in power electronics. The chapter closes with a summary table and the research gaps that motivate this work.

2.2 Vehicle-to-Grid Technology and Grid Services

The foundation of V2G research was laid by Kempton and Tomić, who formulated the capacity and net revenue of V2G power and argued that EV fleets could provide regulation and spinning reserve and eventually support large-scale renewable generation [4], [8]. Han *et al.* designed an optimal V2G aggregator that schedules a fleet for frequency regulation using dynamic programming [12], and Sortomme and El-Sharkawi formulated the optimal scheduling of V2G energy and ancillary services [13]. Review papers by Yilmaz and Krein [14], Tan *et al.* [15] and Habib *et al.* [16] examined the impact of V2G on distribution systems: they report benefits such as peak shaving, valley filling, loss reduction and voltage support, but also challenges such as battery degradation, harmonic injection, protection coordination and the need for bidirectional infrastructure. Shumei *et al.* built and simulated a V2G system inside a micro-grid and noted that V2G is far easier to realise at micro-grid scale than in the general power grid [9].

2.3 Bidirectional EV Chargers

Yilmaz and Krein reviewed charger topologies and power levels and classified chargers as on-board or off-board, unidirectional or bidirectional, and conductive or inductive [6]. Unidirectional chargers are simple but cannot support V2G. Kisacikoglu *et al.* designed a single-phase on-board bidirectional charger and showed that it can supply reactive power to the grid with little effect on the battery [17]. Kesler *et al.* extended this to a three-phase bidirectional off-board charger [18]. Tan *et al.* presented a bidirectional battery charger consisting of an AC–DC converter and a buck–boost DC–DC converter with constant-current and constant-voltage control [19]; this constant-current PI scheme was adopted in the base paper. On-board AC chargers are limited by the size, weight and cost of the converter that must be carried in the vehicle, which is why high-power V2G is better served by off-board DC charging.

2.4 DC Fast-Charging Station Architectures

Arancibia and Strunz modelled a fast DC charging station in which several off-board DC–DC chargers share a common DC bus fed by a grid-connected rectifier/inverter with an LCL filter, and gave a design procedure for the station and filter parameters [20]. Mohammed Shakeel and Malik used this architecture in a micro-grid, added a PV array to the DC bus and demonstrated V2G and G2V operation with

active power regulation [7]. They noted that the station could also provide reactive power and frequency regulation and recommended a supervisory controller for future research. Their controllers, however, were standard PI regulators; the dynamic performance of the station under faster or more demanding control was not studied.

3.SYSTEM DESCRIPTION AND MATHEMATICAL MODELLING

3.1 Introduction

This chapter describes the micro-grid test system and the DC fast-charging station of the base paper [7], and develops the mathematical models of each component used for controller design and simulation: the EV battery, the bidirectional off-board charger, the grid-connected inverter, the LCL filter, the phase-locked loop and the DC link. The chapter ends with the simulation platform and the modelling assumptions.

3.2 Micro-grid Test System

The micro-grid test system is shown in Fig. 3.1 and its ratings are listed in Table 3.1. A 100 kW wind turbine driving a DFIG and a 150 kW resistive load are connected to the 480 V AC bus, which is linked to a 25 kV distribution feeder and a 120 kV equivalent transmission system at the point of common coupling (PCC) through step-up transformers. The DC fast-charging station is connected to the AC bus through a 250 kVA bidirectional GCI. The station's 1.5 kV DC bus interfaces four EV batteries through off-board chargers and a 50 kW PV array through a boost converter with MPPT.

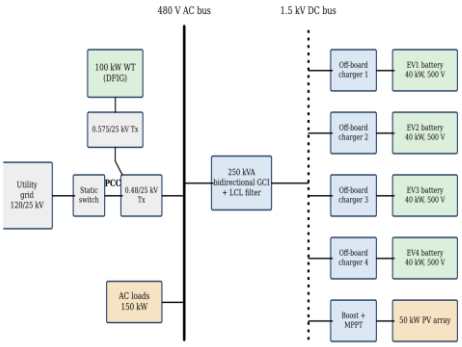


Fig. 3.1 Micro-grid test system with the DC fast-charging station (redrawn after [7])

Table 3.1 Ratings of the micro-grid test system [7]

Case	Purpose	Scenario
1	Base-paper scenario	EV_1: +80 A (V2G) for 1–4 s; EV_2: −40 A (G2V) for 4–6 s (Table I of [7])
2	PV variation	EV_1 +60 A, EV_2 −40 A from 0.3 s; PV ramp 50→30 kW at 1.0–1.2 s, step back to 50 kW at 2 s
3	Multiple EVs	Four EVs with staggered steps (+80, −40, +60, −80 A) between 0.5 s and 2.5 s
4	Parameter variation	Case 1 repeated with C_{dc} −40 %, L +50 %, L_{batt} +50 % and R_s ×2, and all combined
5	Grid voltage sag	20 % sag for 200 ms during 80 A V2G operation
6	Power quality	THD of grid current, switching model, three grid/inverter conditions
7	Benchmark and noise	Optimised PI vs ANN; sensor noise sensitivity

SIMULATION RESULTS AND DISCUSSION

6.1 Introduction

This chapter compares the base-paper PI control with the proposed ANN control through seven case studies, summarised in Table 6.1. Where it is informative, the optimised PI benchmark of Section 5.7.3 is included as a third controller. All averaged-model results include the one-sample computation delay. Unless stated otherwise, the operating conditions follow the base paper: wind power 100 kW, PV power 50 kW, load 150 kW, unity power factor and initial SOC of 50 %.

AMERICAN JOURNAL OF MANAGEMENT AND IOT MEDICAL COMPUTING
Peer Reviewed, Referred & Indexed Journal
E-ISSN: 3069-0110
Vol.5, No.4 (2026)
www.ajmimc.com

Case	Purpose	Scenario
1	Base-paper scenario	EV_1: +80 A (V2G) for 1–4 s; EV_2: −40 A (G2V) for 4–6 s (Table I of [7])
2	PV variation	EV_1 +60 A, EV_2 −40 A from 0.3 s; PV ramp 50→30 kW at 1.0–1.2 s, step back to 50 kW at 2 s
3	Multiple EVs	Four EVs with staggered steps (+80, −40, +60, −80 A) between 0.5 s and 2.5 s
4	Parameter variation	Case 1 repeated with C_{dc} −40 %, L +50 %, L_{batt} +50 % and R_s ×2, and all combined
5	Grid voltage sag	20 % sag for 200 ms during 80 A V2G operation
6	Power quality	THD of grid current, switching model, three grid/inverter conditions
7	Benchmark and noise	Optimised PI vs ANN; sensor noise sensitivity

Table 6.1 Case studies

6.6 Case 5: Grid Voltage Sag

With EV_1 discharging at 80 A, the grid voltage is reduced to 0.8 pu for 200 ms starting at 1.0 s (Fig. 6.12). The sag reduces the power exported for a given i_d, so the DC bus charges until the voltage loop raises i_d. The DC-bus deviation at the start of the sag is 20.5 V with PI and 16.0 V with ANN, and at voltage recovery 21.9 V and 18.3 V; the settling times fall from 8.9 ms and 8.2 ms to 5.3 ms and 4.3 ms. Here the optimised PI performs slightly better than the ANN (14.5 V and 15.8 V).

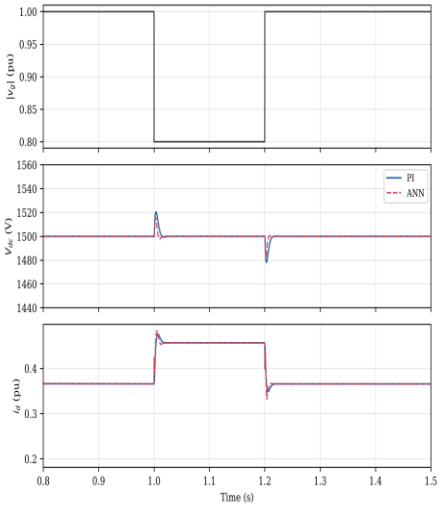


Fig. 6.12 Case 5: grid voltage magnitude, DC-bus voltage and d-axis current during a 20 % grid voltage sag

6.7 Case 6: Power Quality

The THD of the grid-injected current was evaluated with the switching model (Section 3.11), with inverter-side current feedback, at the V2G (0.37 pu) and G2V (0.11 pu) operating points of Case 1. Three conditions were studied: (a) ideal switches and an ideal grid, which corresponds to the conditions of the base paper; (b) 2 µs dead time; and (c) 2 µs dead time plus background grid distortion (2 % fifth and 1.5 % seventh harmonic). The results are listed in Table 6.3, and spectra for conditions (a) and (b) are shown in Fig. 6.13 and Fig. 6.14.

Table 6.3 Case 6: THD of the grid current (%) — limit 5 % [27], [28]

Condition	Point	PI	Opt. PI	ANN	Meets 5 %?
(a) Ideal (base-paper conditions)	V2G	0.74	0.78	1.08	All
(a) Ideal (base-paper conditions)	G2V	2.15	3.03	3.59	All
(b) 2 µs dead time	V2G	4.24	5.76	5.82	PI only
(b) 2 µs dead time	G2V	4.1	3.49	4.66	All
(c) Dead time + distorted grid	V2G	9.69	12.46	12.56	None
(c) Dead time + distorted grid	G2V	23.53	23.95	27.24	None

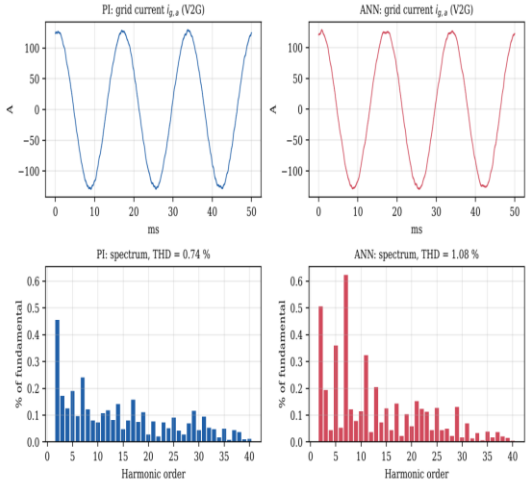


Fig. 6.13 Case 6(a): grid current and harmonic spectrum during V2G, ideal conditions

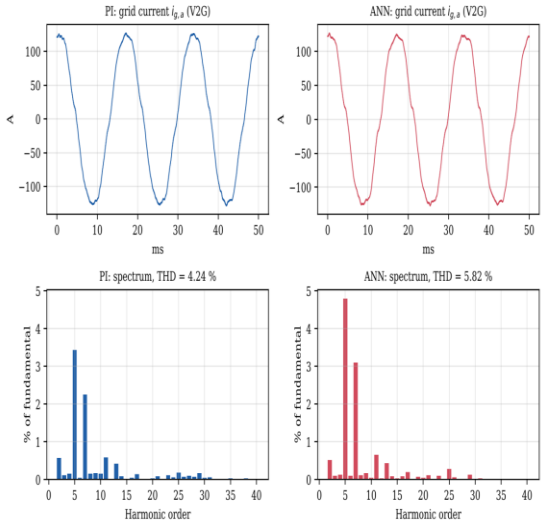


Fig. 6.14 Case 6(b): grid current and harmonic spectrum during V2G with 2 µs dead time

Under the conditions of the base paper both controllers easily meet the 5 % limit. The base paper reported 2.31 % THD; the slightly different value here reflects differences in the inverter model and operating point. The ANN, however, gives consistently *higher* THD than the base PI. With dead time its V2G THD (5.82 %) slightly exceeds the 5 % limit, while the base PI (4.24 %) remains within it. The reason is the low effective gain of the trained dq-current ANN (Fig. 5.10): low-order harmonics caused by dead time (mainly the 5th and 7th) are rejected less strongly. The training cost contained no harmonic term, so the optimiser had no reason to preserve high gain at the 5th and 7th harmonic frequencies. With a distorted grid, none of the controllers meets the limit, which shows that dq-frame PI and ANN current controllers alike need harmonic compensation (for example resonant controllers or dead-time compensation) when the grid voltage itself is distorted.

6.8 Case 7: Benchmark against Optimised PI and Noise Sensitivity

Fig. 6.15 compares the DC-bus transients of the three controllers in Case 1. The optimised PI and the ANN give almost identical responses, both much better than the base PI. The ANN has a 10–90 % battery-current rise time of 0.9 ms against 1.3 ms for the optimised PI and a slightly smaller ITAE over the full run (679 against 718), whereas the optimised PI has lower overshoot and slightly smaller peaks. The optimised PI achieves this with an outer-loop phase margin of only 26° (crossover 150 Hz), compared with 60° for the base PI.

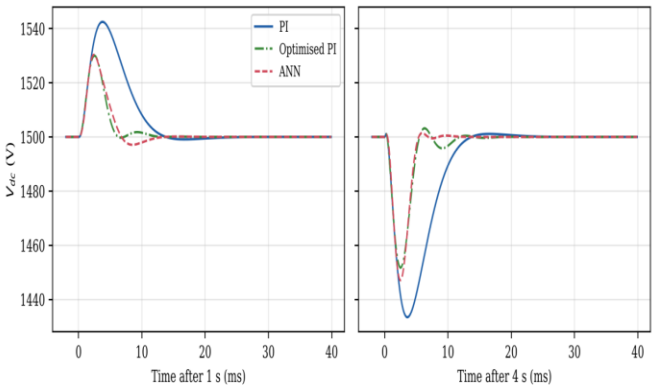


Fig. 6.15 Case 7: DC-bus transients with base PI, optimised PI and ANN

To evaluate noise sensitivity, the steady V2G condition (EV_1 at 80 A) was simulated with sensor noise of 3 V on the DC-bus voltage, 2 A on the grid currents and 1 A on the battery current (Fig. 6.16, Table 6.4).

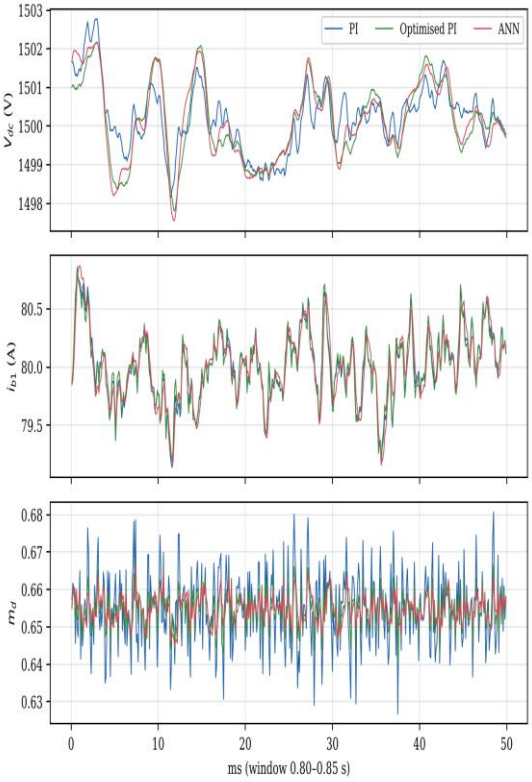


Fig. 6.16 Case 7: DC-bus voltage, battery current and inverter modulation index in steady state with sensor noise

Table 6.4 Case 7: steady-state standard deviations with sensor noise

Quantity	PI	Opt. PI	ANN
DC-bus voltage V_{dc} (V)	0.79	1.02	1
Battery current i_b (A)	0.31	0.3	0.31
Charger modulation index m ($\times 10^{-3}$)	1.8	1.96	1.22
Inverter modulation index m_d ($\times 10^{-3}$)	8.91	4.53	3.53

The ANN produces the least modulation activity of the three controllers: the standard deviation of the inverter modulation index is 60 % lower than with the base PI and 22 % lower than with the optimised PI, and the charger modulation noise is 32 % lower than with the base PI. Lower modulation noise means less switching-ripple variation and less stress on the LCL filter. The price is a slightly larger DC-bus voltage noise (1.00 V against 0.79 V), which remains below 0.07 % of the rated voltage.

6.9 Overall Comparison of PI and ANN Control

The quantitative results are summarised in Table 6.5.

Table 6.5 Comparison of PI and ANN control (Case 1 unless stated)

Performance index	Base PI	Opt. PI	ANN	ANN vs base PI
DC-bus overshoot at V2G start (V)	42.5	30	30.3	−29 %
DC-bus undershoot at V2G→G2V (V)	66.6	48.3	53	−20 %
DC-bus settling time, 1 s / 4 s (ms)	10.1 / 10.6	4.8 / 4.9	5.4 / 4.7	−47 % / −56 %
DC-bus ITAE, full run ($\times 10^{-3}$ V·s²)	1904	718	679	−64 %
Battery current rise time (ms)	1	1.3	0.9	−10 %
Battery current overshoot, EV_1 / EV_2 (%)	10.8 / 10.6	0.2 / 0.9	4.7 / 2.1	−57 % / −80 %
Battery current settling time, EV_1 / EV_2 (ms)	9.7 / 9.8	2.3 / 2.5	2.4 / 2.0	−75 % / −80 %
Steady-state error	0	0	0	—
PV step: peak (V) / settling (ms) (Case 2)	19.0 / 7.6	16.3 / 3.4	15.1 / 3.4	−21 % / −55 %
Multi-EV worst peak (V) / settling (ms) (Case 3)	45.5 / 10.1	32.7 / 4.8	35.0 / 5.5	−23 % / −46 %
Grid sag peak (V) / settling (ms) (Case 5)	20.5 / 8.9	14.5 / 4.4	16.0 / 5.3	−22 % / −40 %
Combined parameter variation, 4 s peak (V) (Case 4)	74.4	61.3	74.4	0%
THD, ideal conditions, V2G (%) (Case 6a)	0.74	0.78	1.08	46%
THD with dead time, V2G (%) (Case 6b)	4.24	5.76	5.82	37%
Inverter modulation noise $\sigma(m_d)$ ($\times 10^{-3}$) (Case 7)	8.91	4.53	3.53	−60 %
Parameters per controller	2	2	51	—
Operations per sample	2 MAC	2 MAC	≈40 MAC + 10 tanh	—

The comparison supports the following conclusions:

- **Dynamic performance.** Compared with the base-paper PI, the ANN reduces DC-bus voltage deviations by 20–29 %, halves the DC-bus settling time, cuts the full-run ITAE by 64 % and reduces battery-current overshoot and settling time by 57–80 %, with no steady-state error.
- **Noise.** The ANN produces the lowest modulation activity of all three controllers.
- **Benchmark.** An optimised PI, tuned on the same objective, achieves nearly the same dynamic performance. The ANN's extra benefit over the optimised PI is small (2–11 % in training cost) and is mainly in battery-current rise time, full-run ITAE and modulation noise. Most of the improvement over the base paper is therefore attributable to closed-loop

optimisation for a delay- and noise-aware objective, rather than to the neural network structure alone.

- **Limitations.** The ANN gives higher grid-current THD than the base PI, and slightly exceeds 5 % with dead time, and its advantage at the V2G→G2V transition disappears under combined parameter variation. Both limitations are consequences of what the training objective did and did not include, and can be addressed by adding harmonic and robustness terms to the training (Chapter 7).

7.CONCLUSIONS AND FUTURE SCOPE

7.1 Conclusions

This thesis extended the V2G DC fast-charging architecture of Mohammed Shakeel and Malik [7] by replacing all PI regulators of the battery chargers and the grid-connected inverter with artificial neural network controllers. The main conclusions are:

1. A reduced-order averaged model of the complete charging station, including one-sample computation delay and sensor noise, reproduced the base-paper results: V2G export of 41.4 kW and G2V import of 21.9 kW, DC-bus regulation at 1500 V with spikes of about 40–65 V, and in-phase/anti-phase grid current in G2V/V2G.
2. A 3–10–1 MLP with error, integral and derivative inputs can replace each PI regulator directly, keeping the original feed-forward, decoupling and modulation stages. Levenberg–Marquardt fitting to the PI law gives a guaranteed-stable starting point, and noise-aware closed-loop optimisation with an evolution strategy then improves the controller.
3. Compared with the base-paper PI, the ANN reduces the DC-bus voltage overshoot from 42.5 V to 30.3 V and the undershoot from 66.6 V to 53.0 V, roughly halves the DC-bus settling time, lowers the full-run ITAE by 64 %, cuts battery-current overshoot from about 11 % to 2–5 %, and lowers the inverter modulation noise by 60 %. These improvements persist with PV variation, multiple EVs and grid voltage sag.
4. A PI controller re-tuned on the same objective achieves nearly the same dynamic performance. The specific benefit of the ANN structure is modest and is seen mainly in faster battery-current rise, slightly lower ITAE and lower modulation noise.
5. The trained ANN gives higher grid-current THD than the base PI, and its advantage at the V2G→G2V transition is lost under combined parameter variation. Under the base-paper conditions all controllers meet the 5 % THD limit of IEEE Std 519/1547.

Overall, the results show that ANN control can significantly improve the transient performance of a V2G fast-charging station relative to the conventional PI design of the base paper, but that a fair assessment must include a re-tuned PI benchmark, digital delay, noise, robustness and power quality.

7.2 Future Scope

- **Robust training.** Train the ANNs on episodes with randomised plant parameters, grid strengths and operating points, to recover the advantage lost under parameter variation.
- **Harmonic-aware training.** Add a harmonic-distortion term to the cost of the current-loop ANN, or combine the ANN with resonant controllers or dead-time compensation, to meet the 5 % THD limit under realistic switching conditions and distorted grids.
- **Recurrent and adaptive networks.** Investigate recurrent ANNs or online adaptation [36], [11] so that the controller can track slow changes in battery and grid parameters.

- **Supervisory control.** Develop the supervisory controller suggested in [7] that dispatches EV current set-points according to SOC, user requirements and micro-grid needs, and extend the station to reactive power and frequency support.
- **Detailed models and hardware.** Validate the controllers in a detailed MATLAB/Simulink model with switching converters, a DFIG and a PV/MPPT model, and then in a hardware-in-the-loop or laboratory prototype.

REFERENCES

[1] International Energy Agency, *Global EV Outlook 2024: Moving Towards Increased Affordability*. Paris, France: IEA, 2024.

[2] R. H. Lasseter, "MicroGrids," in *Proc. IEEE Power Engineering Society Winter Meeting*, New York, NY, USA, 2002, vol. 1, pp. 305–308.

[3] N. Hatziargyriou, H. Asano, R. Iravani, and C. Marnay, "Microgrids," *IEEE Power Energy Mag.*, vol. 5, no. 4, pp. 78–94, Jul./Aug. 2007.

[4] W. Kempton and J. Tomić, "Vehicle-to-grid power fundamentals: Calculating capacity and net revenue," *J. Power Sources*, vol. 144, no. 1, pp. 268–279, 2005.

[5] SAE International, *SAE J1772: SAE Electric Vehicle and Plug-in Hybrid Electric Vehicle Conductive Charge Coupler*, Warrendale, PA, USA, 2017.

[6] M. Yilmaz and P. T. Krein, "Review of battery charger topologies, charging power levels, and infrastructure for plug-in electric and hybrid vehicles," *IEEE Trans. Power Electron.*, vol. 28, no. 5, pp. 2151–2169, May 2013.

[7] F. Mohammed Shakeel and O. P. Malik, "Vehicle-to-grid technology in a micro-grid using DC fast charging architecture," in *Proc. IEEE Canadian Conf. Electrical and Computer Engineering (CCECE)*, Edmonton, AB, Canada, 2019, pp. 1–4.

[8] W. Kempton and J. Tomić, "Vehicle-to-grid power implementation: From stabilizing the grid to supporting large-scale renewable energy," *J. Power Sources*, vol. 144, no. 1, pp. 280–294, 2005.

[9] C. Shumei, L. Xiaofei, T. Dewen, Z. Qianfan, and S. Liwei, "The construction and simulation of V2G system in micro-grid," in *Proc. Int. Conf. Electrical Machines and Systems (ICEMS)*, Beijing, China, 2011, pp. 1–4.

[10] B. K. Bose, "Neural network applications in power electronics and motor drives—An introduction and perspective," *IEEE Trans. Ind. Electron.*, vol. 54, no. 1, pp. 14–33, Feb. 2007.